Lasers in Manufacturing Conference 2023

Adjustment of the cutting front and kerf by means of beam shaping to increase the speed of laser cutting

Jannik Lind[a,b,*], Christian Hagenlocher[a], Niklas Weckenmann[c], David Blazquez-Sanchez[c], Clemens Ackermann[b], Rudolf Weber[a], Thomas Graf[a]

[a]*Institut fuer Strahlwerkzeuge (IFSW), University of Stuttgart, Pfaffenwaldring 43, 70569 Stuttgart, Germany*
[b]*Research Campus ARENA2036, Pfaffenwaldring 19, 70569 Stuttgart, Germany*
[c]*Precitec GmbH & Co. KG, Draisstraße 1, 76571 Gaggenau, Germany*

Abstract

The shape of the laser beam significantly influences the geometry of both the cutting front and the cutting kerf. The angle of the cutting front impacts the absorptivity while the width of the kerf defines the amount of material, which must be molten. The kerf´s geometry therefore determines the maximum possible cutting speed. These relations between absorptivity, the width of the kerf, and the maximum cutting speed are described by a simple model in Lind et al., 2023. In order to verify the prediction of the model, the geometry of the interaction zone was observed by means of X-ray imaging. The results show an increase of absorptivity in case of an enlargement of the beam in the direction of the feed, while the cross-sectional area of the kerf increases in case of an enlargement of the width of the beam in the transversal direction.

Keywords: Laser beam cutting; beam shaping; online high-speed X-ray imaging; maximum cutting speed

1. Introduction

The average laser power of solid-state lasers has increased significantly over the past few years. This allows for cutting thicker sheets, as shown by Wandera and Kujanpää, 2011 and Wandera et al., 2009. However, this

* Corresponding author. Tel.: +49 160 91294149
E-mail address: jannik.lind@arena2036.de

development has led to increased complexity in adjustable process parameters and laser beam properties to optimize cut quality and cutting speed, as described by Pocorni et al., 2018.

The maximum cutting speed is achieved when the absorbed power is insufficient to melt the material volume which would be required to generate a cutting kerf, as described in Steen and Mazumder, 2010 and Hügel and Graf, 2009. The amount of absorbed power is determined by the absorptivity of the laser beam on the material surface, while the amount of molten material per unit of time depends on the cross-sectional area of the kerf and the cutting speed. The beam's caustic determines the cross-sectional area of the kerf, as shown by Vasileska et al., 2022 and Goppold et al., 2014. It was observed that the cross-sectional area of the kerf is enlarged and that the maximum cutting speed is reduced, when the diameter of the beam is increased. Moreover, the diameter of the beam affects the absorptivity at the cutting front, as shown by Mahrle and Beyer, 2009. The geometric model of the cutting front presented by Mahrle et al. shows that the absorptivity increases with an increasing beam diameter up to the Brewster angle resulting in a higher maximum cutting speed. However, increasing the beam diameter also enlarges the cross-sectional area of the kerf, which has a contrary impact on the maximum cutting speed. Therefore, an analytical and experimentally verified model is necessary in order to predict the maximum cutting speed for different beam shapes.

This paper presents a space- and time-resolved experimental X-ray analysis of the influence of different beam shapes on the geometry of the cutting front and the kerf. The relations between absorptivity, the width of the kerf, and the maximum cutting speed are described by an analytical model. The calculated predictions are in good agreement with experimental results.

2. Theory

An analytical approach to estimate the maximum cutting speed for fusion cutting is to consider the energy balance, as described by Steen and Mazumder, 2010 and Hügel and Graf, 2009. With a given maximum laser power P the maximum cutting speed

$$v_{max} = \frac{P \cdot A - P_{L,s} \cdot s}{F \cdot \rho \cdot \left(c_p \Delta T_P + h_S\right)} \tag{1}$$

is obtained by solving the energy balance for laser beam fusion cutting for v. F is the cross-sectional area of the cutting kerf, ρ the density of the cut material, c_p its specific heat capacity, ΔT_P the difference between the temperature of the ejected melt and the ambient temperature, and h_S the latent heat of fusion. The power which is lost by heat conduction depends on the thermal properties of the material as well as the cutting speed and may be expressed by the cutting depth *s* of the workpiece and the depth-specific power loss $P_{L,s}$, as shown by Petring, 1995. Approximating the cutting front by an inclined plane and neglecting multiple reflections in the kerf, the absorptance η_A equals the absorptivity $A = A(\lambda, \theta)$, which depends on the applied wavelength λ, the angle of incidence θ, the processed material and its temperature. The absorptivity is determined by the Fresnel equations, as presented by Demtröder, 2016.

Fig. 1. sketches the geometrical conditions in the kerf with the average global inclination of the cutting front, as indicated by the blue dashed line. The caustic of the beam is sketched by the red lines, where d_f is the diameter of the beam waist. It is assumed that the length of the cutting front equals the extent of the beam's cross-section in the direction of the feed at maximum cutting speed. With the definition of the inclination angle of the cutting front as shown in Fig. 1., the average inclination angle $\theta_{@vmax}$ also equals the average angle of incidence of the beam on the cutting front at maximum cutting speed. Fig. 1b. illustrates the conditions with an increased beam diameter d_{f2} compared to the beam diameter d_{f1} in Fig. 1a. According to Mahrle and Beyer, 2009 the diameter of the beam determines the global angle of incidence

$$\theta_{@vmax} = arctan\left(\frac{s}{\frac{d(z=0)}{2} + \frac{d(z=s)}{2}}\right), \tag{2}$$

where s is the thickness of the sheet and $d(z)$ is the beam diameter at the distance z from the top surface of the sheet.

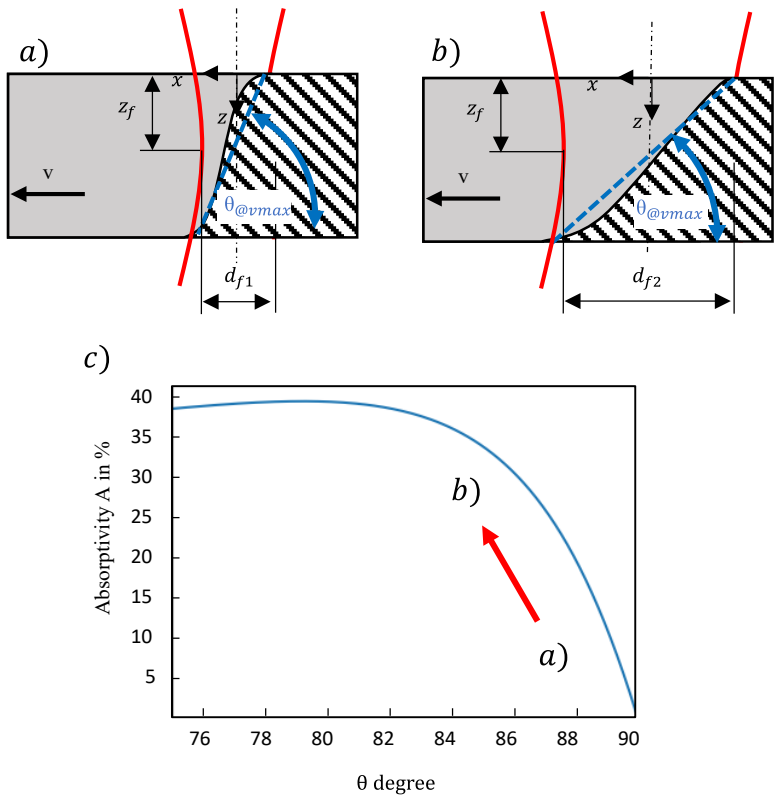

Fig. 1. The global angle $\theta_{@vmax}$ describes the average inclination of the cutting front and equals the averaged angle of incidence of the beam on the cutting front at maximum cutting speed. The waist of the beam is located at the distance z_f from the top surface of the cut sheet. Fig. 1c. shows the absorptivity as a function of the angle of incidence assuming liquid iron and unpolarized radiation with a wavelength of 1030 nm as calculated using Fresnel's equations.

The averaged angle of incidence on the cutting front can be used to calculate the absorptivity $A = A(\theta)$ using the Fresnel equations. Assuming an unpolarized beam with a wavelength of 1030 nm, Fig. 1c. shows the absorptivity as a function of the angle of incidence on a surface of liquid iron with the complex refractive index $n_c = 3.6 - 5.0i$ [17, 18]. With the geometric assumption that the length of the cutting front equals the extent of the beam's cross-section in the direction of the feed at maximum cutting speed, it follows from equation (2) that an increased extent of the beam's cross-section (Fig 1b.) is associated with a reduced angle of incidence θ and hence an increased absorptivity A as long as θ exceeds approximately 80°, as shown in Fig. 1c. With an

increased absorptivity A, the maximum cutting speed v_{max} is increased according to equation (1). Considering the geometrical conditions of the beam´s cross-section in the plane normal to the feed, as sketched in Fig. 2., we made in Lind et al., 2023 the basic assumption that the cross-sectional area of the cutting kerf corresponds to the area

$$F = \int_{z=0}^{z=s} \left(d_f \cdot \sqrt{1 + \frac{(z - z_f)^2}{z_R^2}} \right) dz \tag{3}$$

covered by the caustic of the beam in the y-z plane from the top to the bottom surface of the sample.

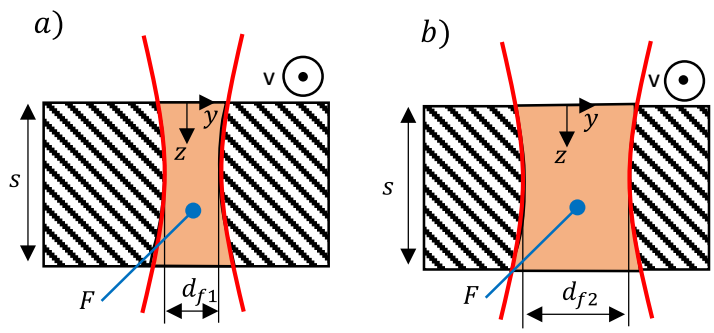

Fig. 2. Cross-sectional area of the cutting kerf for different beam diameters.

An increased extent of the beam's cross-section in the y-z plane as indicated in Fig 2b. results in an increased cross-sectional area of the cutting kerf F, which reduces the maximum cutting speed v_{max} according to equation (1). It follows from equation (2) and equation (3) that the diameter of the beam $d(z)$ influence both the cross-sectional area of the kerf F and the absorptivity A which results from the changed inclination angle of the front. According to equation (1), both quantities influence the maximum cutting speed that can be achieved with a given laser power P.

3. Experimental Setup

Fusion cutting of stainless steel 1.4301 was investigated using a Trudisk8001 laser with a wavelength of 1.03 µm in combination with two different cutting heads from Precitec in order to verify the prediction of the model given by the equations (1), (2) and (3). A sketch of the experimental setup is shown in Fig. 3a. The origin of the cartesian coordinate system was set at the intersection point of the centerline of the nozzle and the surface of the sample. The feed was achieved by moving the sample in x direction.

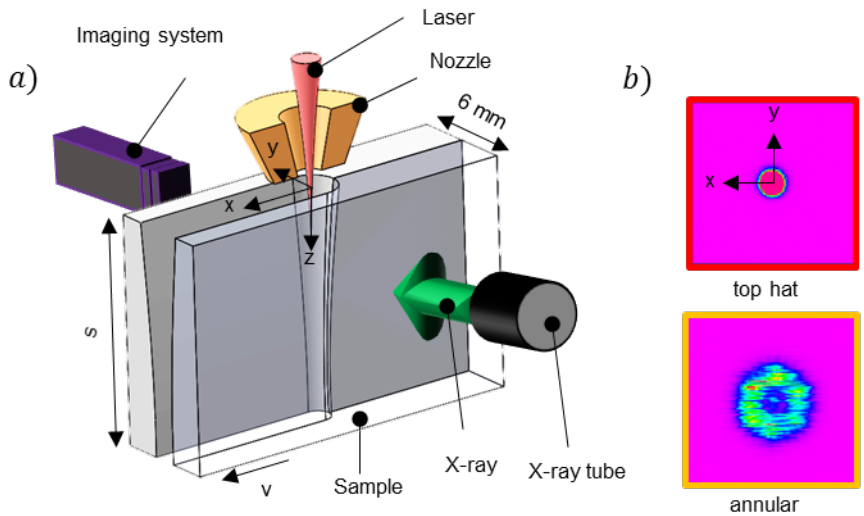

Fig. 3. Sketch of the experimental setup a) and intensity distributions in the focal plane b).

The X-ray imaging system consists of a tube emitting X-rays (green) that transirradiate the sample and of an imaging system (purple), which consists of a scintillator, an image intensifier, and a high-speed camera, as described in Abt et al., 2011 and Lind et al., 2019. The high-speed camera was used to capture images of the process at a frame rate of 1000 fps with a spatial resolution of 37 pixels/mm. The acceleration voltage of the X-ray tube was set to 140 kV at a tube power of 90 W. The width of the samples in y-direction was chosen to be 6 mm to allow for a suitable X ray imaging. The X ray videos were post-processed with a flat-field correction and Kalman filtering in order to enhance the image contrast and to reduce the noise, as shown in Kalman, 1960. In order to avoid overexposure of the X-ray camera above and below the sample, lead apertures were positioned at the upper and lower edge of the sample.

Fig. 3b. shows the intensity distributions of the two laser beams in the focal plane. The waist diameter d_f, the Rayleigh-length z_r and the beam propagation factor M^2 were calculated using the 2nd order moments. The beam shape which we refer to as “top hat” in the following was obtained by connecting a *ProCutter2.0* cutting head to a beam-delivery fiber with a core diameter of 100 µm and by focusing the beam to a waist diameter of approximately $d_f \approx 166\ \mu m$, a Rayleigh-length of about $z_r \approx 1.6\ mm$, and a beam propagation factor of $M^2 \approx 13$ as measured with a Primes *HighPower MicroSpotMonitor*. Due to the fiber-optic beam delivery the beam exhibited a top-hat shaped intensity distribution at the waist.

To obtain the beam shape referred to as “annular”, a *ProCutterEdgeTec* cutting head was connected to a beam-delivery fiber with a core diameter of 100 µm and the beam was focused to a waist with an outer diameter of approximately $d_f \approx 900\ \mu m$ with an annular shaped intensity distribution, a Rayleigh-length of about $z_r \approx 8.3\ mm$, and a beam propagation factor of $M^2 \approx 74$ according to measurements with a Primes *Focus Monitor*. The influence of the shape of the laser beam on the geometries of the cutting front and the kerf was investigated by analyzing cuts with a length of 40 mm. The laser power *P*, the distance between the nozzle and the sample´s surface, the diameter of the nozzle, the cutting speed *v*, the pressure of the nitrogen processing gas, and the waist position were adapted in order to achieve the maximum cutting speed.

4. Results

The grey-scale value of each pixel from the obtained X-ray images contains information about the thickness of the irradiated material and therefore of the width of the cutting kerf. Fig. 4a. and Fig. 4b. show the 3D-geometry of the cutting kerf that was reconstructed from this information in different views at maximum cutting speed. The reconstruction method is based on the Lambert-Beer-Law and assumes a mirror symmetrical geometry of the kerf to the x-z plane, as described in Lind et al., 2020. Connecting the front of the kerf at the top surface with the one at the bottom surface of the sample (red dashed line) delivers the experimentally determined angle θ_{exp} which corresponds to the average angle of incidence of the radiation on the cutting front. The cross-sectional area of the front view in the y-z plane is the experimentally determined cross-sectional area F_{exp} of the kerf, as highlighted by the gray dotted lines in Fig. 4.

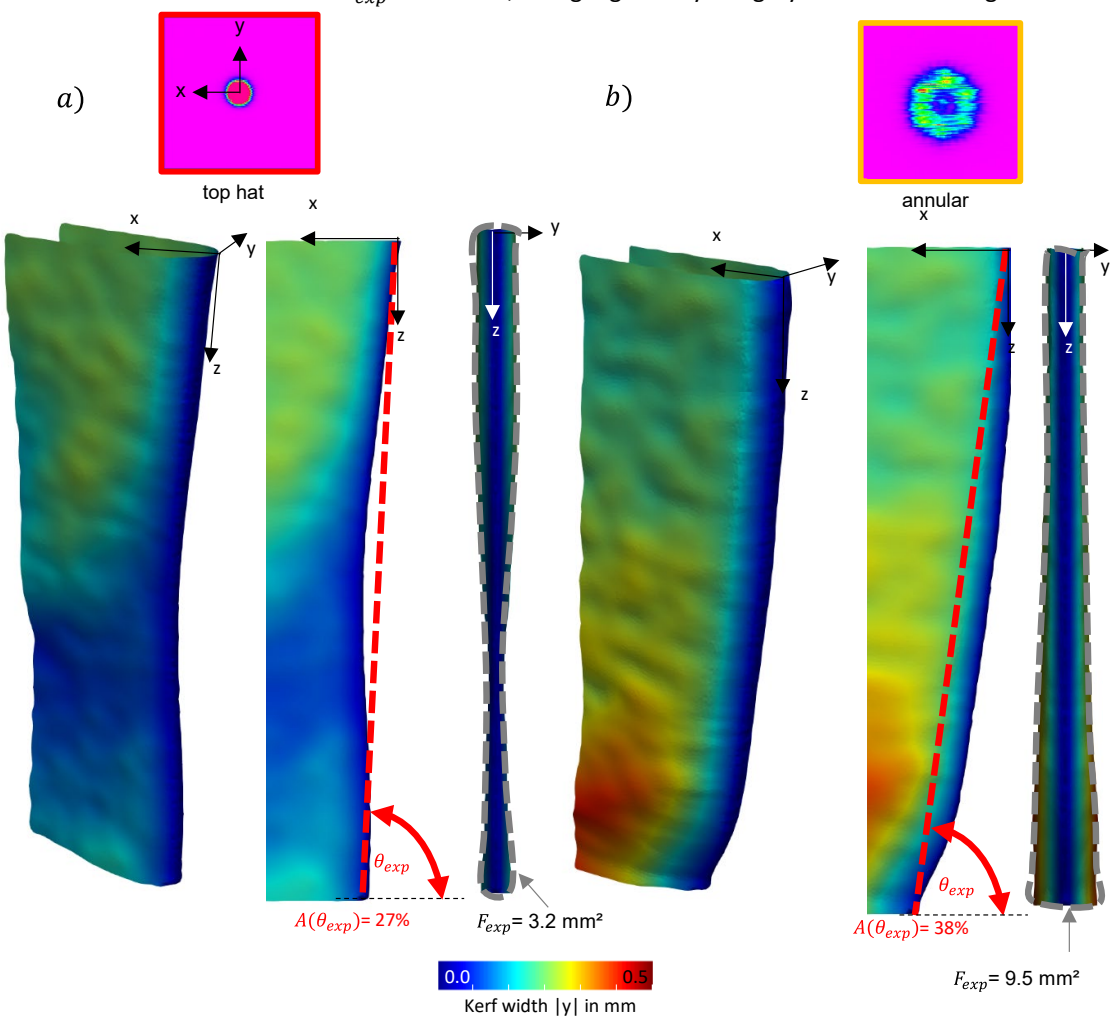

Fig. 4. Isometric view of the 3D reconstruction of the kerf and the cutting front of the beam shape a) “top-hat” and b) “annular” at maximum cutting speed.

Fig. 4. shows that the experimentally determined area F_{exp} of the beam shape “annular” is three times larger than the area of the beam shape “top hat”. It can be seen in Fig 4. that the experimentally determined global angle of incidence θ_{exp} of the laser beam on the cutting front for the beam shape “top hat” is increased compared to the angle on the cutting front for the beam shape “annular”. Thus, the absorptivity for the beam “annular” was increased by 40% compared to the absorptivity achieved with the beam shape “top hat”.

Increasing the diameter of the beam decreases the angle of incidence which leads to an increased absorptivity for angles of incidence ranging between 90° and approximately 80°, as shown in Fig. 1c. Increasing the diameter of the beam however also enlarges the cross-sectional area of the kerf, which has a contrary impact on the maximum cutting speed. While an increased absorptivity increases the maximum cutting speed according to equation (1), the cutting speed is reduced by an enlarged cross-sectional area of the kerf. Inserting the material properties of stainless steel, the equations (3) and the absorptivity *A* from equation (2) allows the calculation of the maximum cutting speed v_{max}. The material properties and the value of the depth-specific power loss are listed in Lind et al., 2023. Fig. 5. shows the comparison of the experimentally determined maximum cutting speed $v_{max,exp}$ (crosses), as presented in Lind et al 2023, and predicted maximum cutting speed v_{max} (solid lines), as calculated by equation (1). The maximum cutting speed is presented as a function of the laser power P for the two different shapes of the laser beam. The scatter band (shaded area) of the predicted maximum cutting speed v_{max} represents a deviation of the measured beam propagation factor M² by $\pm$ 15%.

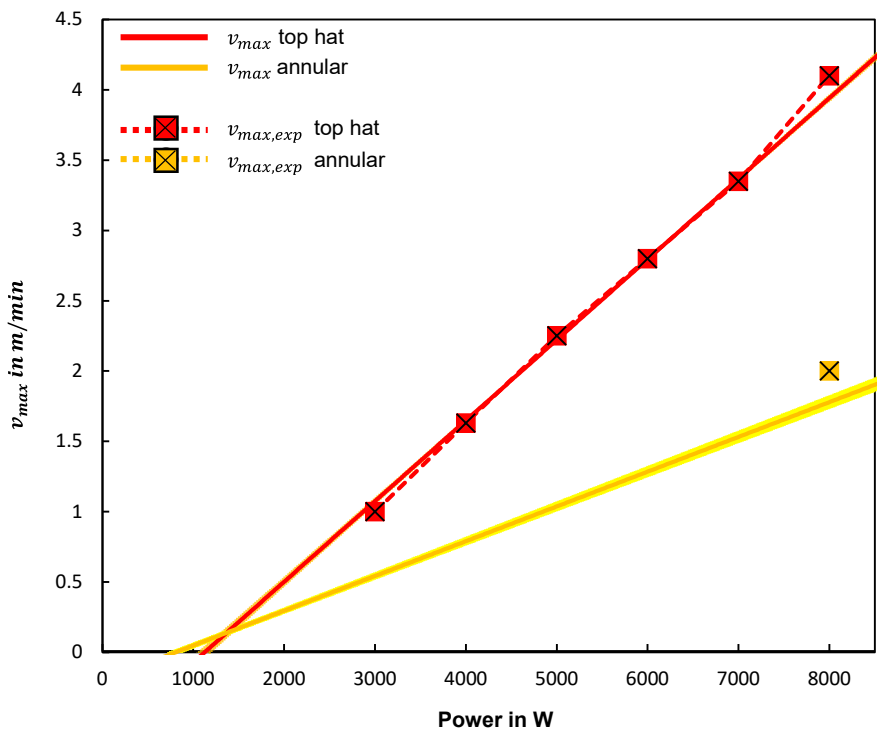

Fig. 5. Experimentally determined maximum cutting speed $v_{max,exp}$ and calculated maximum cutting speed v_{max} as a function of the laser power *P* for two different beam shapes.

As expected, the results show that the maximum cutting speed increases with increasing laser power *P.* The results show that at the same laser power of 8 kW the beam shape “top hat” allowed to attain the higher

maximum cutting speed. As shown before, the beam shape “annular” leads to the higher absorptivity but also to a significantly enlarged cross-sectional area of the cutting kerf as compared to the results obtained with the “top hat” beam. This results in a reduced maximum cutting speed, as predicted by equation (1). The good agreement between the measured and calculated results proves that the calculated cross-sectional area F, angle of incidence $\theta_{@vmax}$ and hence the absorptivity $A(\theta_{@vmax})$ can be used to predict the maximum cutting speed v_{max} according to equation (1) for different shapes of the laser beam.

Conclusion

The model of Lind et al., 2023 was validated by a space- and time-resolved experimental X-ray analysis for two different shapes of the laser beam. The experiments show the influence of the beam shape on the geometry of the cutting front and the kerf. The good agreement between the measured and calculated results proves that the simple analytical model is a valuable tool to predict the maximum cutting speed for different shapes of the laser beam.

Acknowledgements

This research was supported by Precitec GmbH & Co. KG. The laser beam source TruDisk8001 (DFG object number: 625617) was funded by the Deutsche Forschungsgemeinschaft (DFG, German Research Foundation) – INST 41/990-1FUGG.

References

Abt F., Boley M., Weber R., Graf T., Popko G., Nau S., 2011. Novel X-ray System for in-situ Diagnostics of Laser Based Processes – First Experimental Results. Physics Procedia 2011, pp 761–770. doi: 10.1016/j.phpro.2011.03.095

Demtröder W., 2016. Experimentalphysik, Atome, Moleküle und Festkörper

Goppold C., Zenger K., Herwig P., Wetzig A., Mahrle A., Beyer E., 2014. Experimental Analysis for Improvements of Process Efficiency and Cut Edge Quality of Fusion Cutting with 1µm Laser Radiation. Physics Procedia 56, pp 892–900. doi: 10.1016/j.phpro.2014.08.108

Hügel H., Graf T. (2009). Laser in der Fertigung. Vieweg+Teubner, Wiesbaden

Kalman R. E., 1960. A New Approach to Linear Filtering and Prediction Problems. Journal of Basic Engineering 82, pp 35–45. doi: 10.1115/1.3662552

Lind J., Blazquez-Sanchez D., Weidensdörfer J., Weber R., Graf T., 2019. High-speed X-Ray Imaging of the Cutting Process during Laser Beam Cutting of Aluminum. Lasers in Manufacturing Conference. doi: 10.2351/1.4983261

Lind J., Fetzer F., Hagenlocher C., Blazquez-Sanchez D., Weber R., Graf T., 2020. Transition from Stable Laser Fusion Cutting Conditions to Incomplete Cutting Analysed with High-speed X-ray Imaging. Journal of Manufacturing Processes 60, pp 470–480. doi: 10.1016/j.jmapro.2020.10.068

Lind J., Hagenlocher C., Weckenmann N., Blazquez-Sanchez D., Weber R., Graf T., 2023. Adjustment of the geometries of the cutting front and the kerf by means of beam shaping to maximize the speed of laser cutting. Int J Adv Manuf Technol 126, pp 1527–1538. doi: 10.1007/s00170-023-11215-5

Mahrle A., Beyer E., 2009. Theoretical aspects of fibre laser cutting. J. Phys. D: Appl. Phys. 42, p 175507. doi: 10.1088/0022-3727/42/17/175507

Petring D., 1995. Anwendungsorientierte Modellierung des Laserstrahlschneidens zur rechnergestützten Prozessoptimierung. Dissertation, RTWH-Aachen

Pocorni J., Powell J., Frostevarg J., Kaplan A. F., 2018. The geometry of the cutting front created by Fibre and CO2 lasers when profiling stainless steel under standard commercial conditions. Optics & Laser Technology 103, pp 318–326. doi: 10.1016/j.optlastec.2018.01.055

Steen W. M., Mazumder J. (2010). Laser Material Processing. Springer London, London

Vasileska E., Pacher M., Previtali B., 2022. In-line monitoring of focus shift by kerf width detection with coaxial thermal imaging during laser cutting. Int J Adv Manuf Technol 118, pp 2587–2600. doi: 10.1007/s00170-021-07893-8

Wandera C., Salminen A., Kujanpaa V., 2009. Inert gas cutting of thick-section stainless steel and medium-section aluminum using a high power fiber laser. Journal of Laser Applications 21, pp 154–161. doi: 10.2351/1.3184429

Wandera C., Kujanpää V., 2011. Optimization of parameters for fibre laser cutting of a 10 mm stainless steel plate. Proceedings of the Institution of Mechanical Engineers, Part B: Journal of Engineering Manufacture 225, pp 641–649. doi: 10.1177/2041297510394078